scientific reports

Check for updates

OPEN

Evolutionary optimisation of pixelated IFA inspired antennas

Dominik Mair✉ & Daniel Baumgarten

As wireless communication systems increasingly require compact and efficient antennas, conventional antenna design methods are proving difficult to meet the rigorous demands of modern applications. For this purpose, this study introduces a methodology which uses pixelated Inverted-F Antenna (IFA) inspired designs optimised through genetic algorithms to enhance performance in constrained spatial environments. As pixels the antenna features the exemplary use of Einstein Hat-shaped tiles, enabling the antenna to efficiently utilize space. A with the proposed method optimised antenna is compared to traditional IFA designs and shows improved properties like enhanced antenna gain and efficiency as well as smaller reflection coefficient offering a promising solution for future compact antenna systems in the Internet of Things and beyond. Finally, a prototype was manufactured and the scattering parameters and antenna gain were measured within an anechoic chamber.

In the landscape of modern communication systems, antennas tailored for specific applications and environmental contexts are crucial. These systems often demand compact antennas to fulfil on the one hand space constraints of various applications and the other hand feature high efficiency. When dealing with limited space, one might consider employing communication technologies operating at higher frequencies to mitigate space constraints. However, this solution introduces its own set of challenges: path losses increasing with the square of the frequency and the complexities of multi-path propagation, which lower the performance of e.g. Internet of Things (IoT) applications[1]. Also, the IoT can not only necessitate long communication ranges but also depend on specific technologies like 2.4 GHz WiFi, Bluetooth, Thread and Zigbee which are pivotal for achieving technological interoperability within the IoT ecosystem.

In the realm of IoT, the miniaturization of antennas leads to the development of smaller devices. Nonetheless, this miniaturization often results in lower efficiency and bandwidth, which can, in turn, reduce communication distances or require higher power for a fixed specified distance to maintain performance.

Addressing these design challenges, the evolution of antenna technology over recent decades has led to significant advancements. Miniaturization methods such as inductive, capacitive, and dielectric loading as well as fractalization, metamaterials, and pixelation have been explored, alongside artificial intelligence with techniques like genetic optimisation (GA), binary particle swarm optimisation (BPSO), and neural networks[2–4].

In this context, pixelated antennas emerge as an exciting area of focus. Characterized by their modular design of discrete "pixels", this approach leads to an enhanced design and optimisation with fast iterations and minimal human input. Most often these pixels are rectangular, hexagonal, or cross-shaped. By harnessing various optimisation algorithms and employing state-of-the-art manufacturing techniques like additive manufacturing, it is possible to engineer antennas with tailored radiation patterns, enhanced efficiency, and expanded operational bandwidths.

Moreover, the design process can be fully autonomous with a comparably low design time of a few hours to days. This convergence enables designers to overcome the limitations of traditional antenna design methods, facilitating a broad exploration of potential configurations. This intelligent, automated design process not only accelerates development but also reveals antenna structures that may have remained undiscovered through conventional means.

The distinctive adaptability of pixelated antennas is among their most notable attributes. This design philosophy grants engineers the ability to fine-tune antenna characteristics to meet the exact requirements of a wide variety of applications, from telecommunications to sensor networks. Such precise control over performance parameters like impedance matching, gain, and directivity is essential for the efficiency and reliability of wireless communication systems.

Additive manufacturing, particularly through laser powder bed fusion (LPBF), has transformed the fabrication of pixelated antennas, enabling complex three-dimensional voxelated structures previously unattainable with conventional methods[5]. This advancement broadens the scope for embedding antennas in various devices, accommodating intricate shapes or tight spaces.

Universität Innsbruck, Department of Mechatronics, Innsbruck 6020, Austria. ✉email: dominik.mair@uibk.ac.at

Researchers have employed several optimisation algorithms for optimising pixelated structures. Zechmeister et al.[6] introduced an approach with Binary Ink Stamp Optimisation, showcasing its efficacy across fifteen benchmark functions and benchmarking it against six leading optimisation algorithms including genetic algorithms, Binary Particle Swarm Optimisation, and Binary Covariance Matrix Adaptation Evolution Strategy (BCMAES), among others. Subsequent research has expanded the application of genetic algorithms in the field. In previous work, our group employed various genetic algorithm strategies to enhance antenna designs for structural health monitoring within concrete environments and for three-dimensional voxelated antennas[5,7]. Similarly, Gjokaj et al.[8] utilized genetic algorithms to refine a pixelated patch antenna design, whereas Ranjan et al.[9] employed a binary wind-driven optimisation algorithm to optimise a pixelated metamaterial absorber. Multi-objective BPSO was applied by Li et al.[3] to optimise pixelated patches, and Ghadimi et al.[10] utilized BPSO for reducing mutual coupling between patch antennas. Additional contributions to the field include the use of deep neural network regression models by Jacobs et al.[4] for predicting resonance frequencies of pixelated patches, the generation of a dielectric resonator antenna by Lee et al.[11] using genetic learning particle swarm optimisation, deep learning-based modelling for inverse design by Karahan et al.[12], optimisation of pixelated metamaterial antennas with elite-preserving genetic algorithms by Sun et al.[13], and perturbation sensitivity analysis for designing reconfigurable pixelated patch antennas by Qiao et al.[14]. Marasco et al.[1] used inkjet printing techniques with metamaterials and genetic algorithms to design a flexible pixelated patch antenna.

Until now no study generated topologically optimised pixelated antennas inspired by Inverted-F antennas (IFA). IFAs are widely used in modern communication systems due to their compact size, low profile, and ability to provide good impedance matching. The IFA design originated from an inverted L-antenna, incorporating a shunt stub for impedance matching, which connects the radiating element to the ground plane, thereby reducing the antenna's overall size.[15,16] Although initially developed for missile applications, the IFA's geometry is well-suited for integration into space-constrained environments, making it an ideal choice for mobile and IoT devices. Various optimization techniques have been employed for IFAs in the past to achieve size reduction, such as meandering[17] or implementing electromagnetic band-gaps in the ground plane[18]. Enhancements in bandwidth have been achieved through the optimization of parasitic patches[19], and multi-band capabilities have been introduced using techniques like L-loading[18].

This study presents, for the first time, a method to optimise IFA-inspired pixelated antennas, demonstrating that they can surpass traditional IFA designs. To the best of the authors knowledge, no prior study has addressed the optimisation of IFA-inspired pixelated antennas so far. An exemplary antenna is presented and measurement and simulation results show that the antenna developed with this algorithm achieves higher gain, better efficiency, and superior impedance matching compared to other studies and commercially available antennas of similar size. Furthermore, the proposed concept allows for the future inclusion of nearby materials in the optimisation process, generating an optimal antenna for specific products with minimal human input.

As pixels, Hat-shaped Einstein tiles were used to demonstrate the ability of the optimisation method to employ complex shaped elements. They were discovered in 2023 by Smith et al.[20] and allow the tiling for a plane aperiodically and without any gaps. In contrast to other aperiodic tilings Einstein tiles require only a single tile. The tiling pattern does not repeat itself in any direction, so any simple translation or rearrangement results in a different tiling. This non-repetitive nature leads to a larger solution space for design configurations compared to elements tiling a plane in a regular repeating pattern like hexagons. Additionally, the hat-shaped tile has a more complex outline than a simple hexagon. Its edges and angles allow it to interlock with neighboring tiles in more varied ways, creating intricate local patterns within the tiling. This variability means there are different connection widths to neighboring elements. For example, minimizing losses could encourage the pattern to use larger connections in areas where losses would be highest. Therefore, the local arrangement of tiles can differ throughout the tiling, leading to the emergence of complex shapes and motifs that are not possible with the uniformity of hexagonal tiles. Patterns generated by Einstein tiles should not be mistaken with Fractals because Einstein tile structures do not necessarily exhibit self-similarity across different scales. However, also hexagon shapes, cross shapes and rectangles can be employed with the proposed method.

The antenna developed in this study was optimised with the help of genetic algorithms for a frequency band from 2.39 to 2.493 GHz with a target reflection coefficient of at most − 17 dB. These values were chosen to optimise the antenna with a safety margin for the 2.4 GHz WiFi band. The ground plane's size is 4 cm by 4 cm to fit the electronics of a future wireless passive sensor node in the IoT and the total size of the substrate is 4 cm by 5 cm.

The described algorithm was implemented with Matlab [Version R2023a, The MathWorks, Inc.][21] and CST Studio [Version 2022.05, Dassault Systèmes][22] and all results were cross-checked with Ansys HFSS [Version 2023R2, ANSYS, Inc.][23].

This work is subsequently structured as follows. First, the antenna structure using pixelated Einstein Tiles is presented in section "Tiled antenna". Then the employed genetic algorithm and the fitness function are described in section "Genetic algorithm". Section "Measurement process" gives a brief description of the measurement procedure. In section "Results" the optimised antenna is presented and simulation results like antenna gain, reflection coefficient, efficiency and complex surface current density are examined followed by measurement results of gain and reflection coefficient. The results are discussed and compared to the state of the art. Finally, conclusions are derived and an outlook on future research is given in section "Conclusion and outlook".

Tiled antenna

As a starting point for the optimisation, a rectangular area with the size a times b is filled with Einstein Tiles. The tiles were created with the online generating tool from the authors of the original Einstein Tile study to pre-generate a large layout of Hat-shaped Einstein tiles covering at least the rectangular area[25].

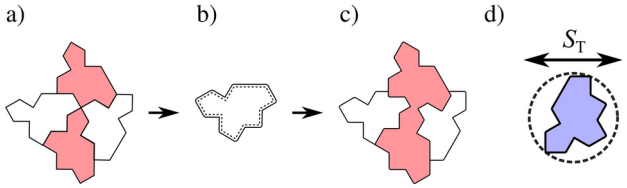

Fig. 1. During the tiling process singularities can occur between two neighbouring Hat-shaped Einstein tiles (coloured in red) as displayed in (**a**). Therefore in (**b**) an outline extension is added with a percentage O_T of the Einstein tiles's size S_T to have well-defined connections. With this concept no singularities occur as shown in (**c**). The definition of a tile's size S_T is seen in (**d**). Software used: Matlab[21], Inkscape[24].

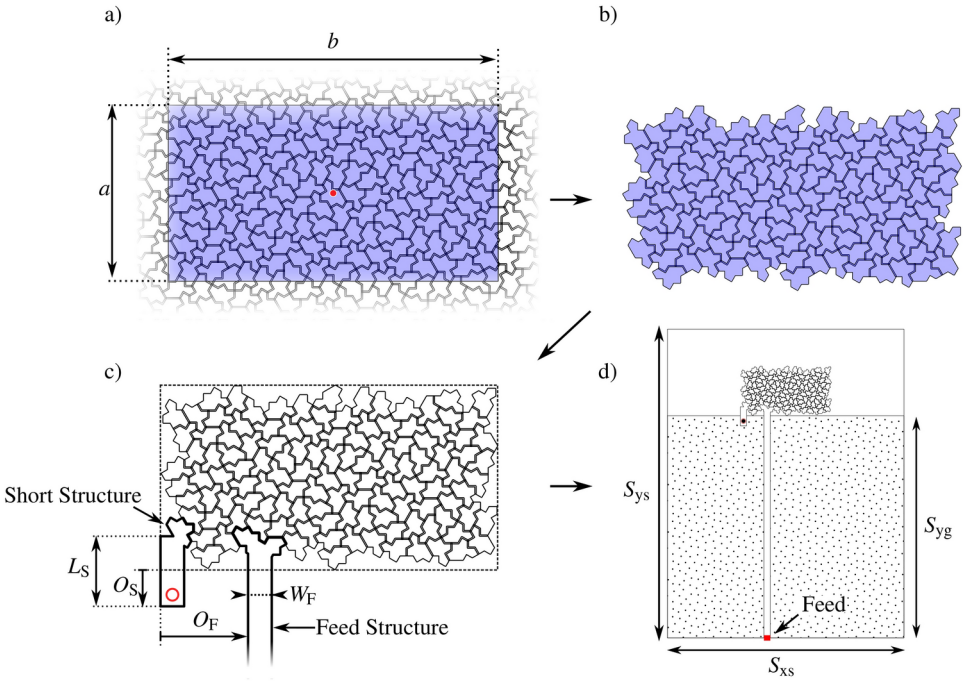

Fig. 2. (**a**) Defines a rectangular area with dimensions a × b overlayed to the pre-generated layout consisting of Hat-shaped Einstein tiles for the tiling process. The red dot marks the centre point. (**b**) Displays the resulting section of tiles, and (**c**) illustrates the addition of the feed and shorting structures. (**d**) Shows the completed initial antenna with tiling, ready for optimisation. Software used: Matlab[21], Inkscape[24].

The size of a single tile (diameter S_T of an enclosing circle) as seen in Fig. 1d is defined by scaling the polygons of the pre-generated layout accordingly. As seen in Fig. 1a, point contacts (singularities) could occur between neighbouring elements, which is why the outline is extended by a percentage O_T of S_T as seen in Fig. 1b. This procedure avoids singularities as seen in Fig. 1c. To tile a predefined area, all tiles that are not completely within a rectangle with a width of *a* and a length of *b* are removed, as shown in Fig. 2a and b.

Afterwards, as seen in Fig. 2c, a short structure with a via toward ground plane (red circle in the figure) is added starting from an offset O_S below the boundary box of the tiled structure. This enables the algorithm to employ short-loading techniques for size reduction. To attach this structure to the antenna, the length of the short structure L_S is incrementally increased starting from O_S in steps of a quarter tile size $S_T/4$ until an intersection with tiles is noticed. Then, a boolean combination combines the intersecting tile with the feed.

The antenna is placed on a substrate with size S_{xs} times S_{ys} as seen in Fig. 2d featuring a ground plane (dotted in the figure) with the size S_{xs} times S_{yg}. The antenna is placed centred regarding its boundary box above the ground plane.

The same procedure as in the generation of the short structure is done for the 50Ω feed structure with the predefined width W_F—depending on thickness and substrate material properties—and predefined offset from the boundary-box of the antenna of O_F. Starting from the feed point originating in the bottom edge of the substrate's ground plane, as seen in Fig. 2d, the length of the feed structure is incrementally increased starting from S_{yg} in steps of a quarter tile size $S_T/4$ until an intersection is noticed. The intersecting tiles are again combined using a boolean union to the feed structure. The feed, as seen in Fig. 2d at the bottom of the antenna, is realized via a CST discrete face port placed between the feed structure and the ground plane.

After this process, the initial antenna is constructed as seen in Fig. 2d and transferred to CST. Every tile is assigned a value in a bitstring, which is either being "0" (non-conducting) or "1" (conducting). This bitstring describes the antenna's conducting elements and therefore its shape and vice versa. By altering this bitstring a binary optimisation—e.g. via binary genetic algorithms—is rendered possible.

Genetic algorithm

In principle, any binary optimisation algorithm, such as those described in the introduction, could be used to optimise an antenna for a specific application. In this study genetic algorithms (GA) are chosen due to their ability to efficiently handle a large number of parameters involved in the proposed antenna design. GAs are widely used and viable options for complex optimisation problems because they can explore a large search space and find sufficient solutions through processes such as selection, recombination, and mutation. The basic steps of the implemented algorithm, as shown in Fig. 3, are described below.

In a first step, an initial population of P randomly generated antennas is defined. To enhance diversity within this population, in our study, we further used the criteria that the individual bitstrings feature a minimum Hamming distance of 16% of the bitstring length to each other. For this purpose, the Hamming distance of a generated antenna to all other already created antennas is computed and the antenna is re-generated until the threshold is met.

Afterwards, these antennas are evaluated based on their cost function, calculated from simulation results. In this study, the following simple cost function is employed:

$$C = \max(20\ \log10(S_{11}(f))) \tag{1}$$

The cost function in Eq. (1) computes the maximum value of the reflection coefficient across the frequencies within the target frequency band. Therefore, a lower cost function value represents a better antenna.

After the cost function values of all antennas in the initial population are calculated, rank-based fitness scaling is applied. It organizes antennas according to their cost function values, awarding lower ranks with elevated fitness scores, whereas antennas with higher ranks are assigned lower fitness scores. This is done by a sorting algorithm assigning the best antenna a rank of 1, the second best a rank of 2 and the worst antenna a rank of P. The fitness value FV is then calculated using the following function:

$$FV = \frac{1}{\sqrt{\text{rank}}} \tag{2}$$

The fitness represents a measure of how well a given antenna performs concerning the cost function.

Thereafter, the E antennas with the highest fitness values (elite individuals) are directly handed on to the next generation followed by selecting antennas either for recombination or mutation to generate the remaining

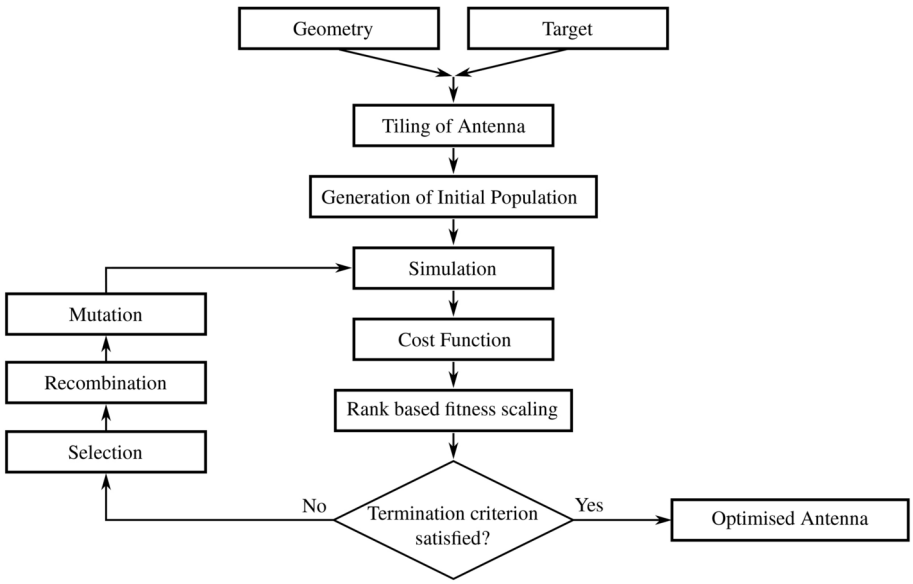

Fig. 3. Flow diagram illustrating the genetic algorithm process used for antenna optimisation. Geometric constants like tile size and antenna size as well as target parameters are defined in Matlab, followed by the pixelation of the antenna structure using Hat-shaped Einstein tiles. An initial population of designs is generated and evaluated using CST Microwave Studio for simulation (frequency domain solver, tetrahedral mesh with refinement). The genetic algorithm iteratively performs mutation, recombination, and selection operations to evolve the antenna designs. After applying rank-based fitness scaling, the process continues until the termination criteria are met, resulting in an optimised antenna configuration. Software used: Inkscape[24].

Property	Value
Population size P	60
Crossover function	Scattered
Crossover rate C	0.5
Mutation function	Uniform
Elite count E	1
Max. generations	300
Min. hamming distance	16 %

Table 1. Parameters used for the genetic algorithm function within Matlab.

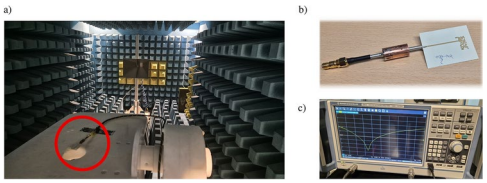

Fig. 4. (**a**) Depicts the antenna under test on a turntable connected via a Balun to a coaxial cable during measurement inside the anechoic chamber. The antenna in the red circle is also displayed in (**b**) with an attached Balun structure. In (**c**) the vector network analyzer is shown, connected to the antenna through feedthroughs into the anechoic chamber, displaying the measured reflection coefficient S_{11}.

$P - E$ antennas. To know how many antennas need to be selected one has to examine further parameters. The adjustable parameter "crossover rate" C dictates the percentage of how many individuals are generated for the new generation via recombination. Because for recombination two antennas are needed, $2(P - E)C$ antennas need to be selected for crossover. Another $(P - E)(1 - C)$ antennas are needed for a mutation to have a population size of P antennas in the next generation. Therefore, in total $K = (P - E)(C + 1)$ have to be selected. These antennas are selected by stochastic universal sampling (SUS). With SUS each antenna is allocated a segment on a line proportional to its fitness value within the total fitness F, starting from a random point r $\in$ [0, F/K] and selecting K antennas at equidistant steps of F/K. Due to this technique an intuitive estimation E_i of how often an antenna i with a fintess of FV_i will be selected can be calculated by:

$$E_i = \frac{FV_i}{F/K} \tag{3}$$

This means the higher the fitness value FV of an individual, the higher the probability of an antenna to be selected and the higher is the chance of an antenna to be selected multiple times.

The selected antennas are then randomly permutated to avoid locality effects and queued in a list for recombination. In the recombination process, the first two antennas in this list are recombined with the help of a randomly created bitstring. The process is continued for antennas 3 and 4 and so on until $(P - E)C$ antennas are created. The remaining antennas in the list are uniformly mutated. This leads to a new generation with P antennas. Afterwards, the whole process is iteratively repeated by simulating the antennas and continually calculating their cost function and fitness values until a termination criterion for one antenna—such as a fulfilled target for the cost function—is satisfied.

The maximum within the cost function in Eq. (1) is chosen instead of the mean or any other function, as this ensures, that the whole frequency band is optimised equally, without preferring frequencies with a reflection coefficient lower than the defined target.

Rank-based fitness scaling is used as it prevents extraordinary antennas (with significantly lower cost function values than the rest of the population) from dominating a substantial proportion of the finite population, which could lead to premature convergence[26]. Equation (2) is used for calculating FV from the *rank* because it amplifies the selection pressure on the most promising individuals, increasing their probability of being selected as parents, while also giving lower-ranked individuals a fair chance of being selected, thus promoting genetic diversity. Such an approach can accelerate the convergence rate of the genetic algorithm, thereby optimising the search efficiency within the solution space.

In this study the parameters shown in Table 1 are used for the genetic algorithm. Note that these hyper-parameters are not thoroughly tuned, but still lead to a successful optimisation.

Measurement process

The resulting antenna, described in section "Results", was validated with measurements of the reflection coefficient $S_{11}(f)$ and antenna gain at 2.45 GHz. For this purpose, the fabricated antenna, along with an attached Balun, was placed on a turntable inside an anechoic chamber, which can be seen in Fig. 4a and b. All measurements were obtained with a VNA [ZNB8, Rohde &Schwarz] as depicted in Fig. 4c. As will be shown in

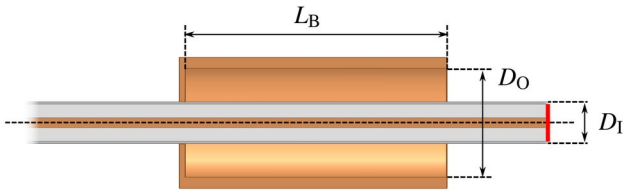

Fig. 5. Sleeve balun with length L_B, inner diameter of the copper pipe D_O and outer diameter of the semi-rigid coaxial cable D_I. Software used: Ansys[23], Inkscape[24].

Property	Value
a	15.3 mm
b	8.3 mm
S_{xs}	40 mm
S_{ys}	50.1 mm
S_{yg}	40 mm
O_s	5.9 mm
O_F	4 mm
W_F	1.081 mm
S_T	1.5 mm
O_T	2%

Table 2. The geometric parameters established before the optimisation process are delineated in Figs. 1 and 2. Furthermore, as noted in the caption of Fig. 1, the factor O_T represents the proportion by which the tile size S_T is extended, expressed as a percentage of S_T.

the section "Results", the final generated antenna has a relatively small ground plane compared to the wavelength i.e. the largest dimension is smaller than half a wavelength and as stated by e.g. Massey et al. especially for small antennas a coaxial feed—needed for the connection of the microstrip line of the antenna to the VNA—couples with the antenna under tests (AUT) currents therefore affecting antenna match and radiation[27].

As further explained by Icheln et al.[28], surface current leaks are the cause of measurement problems, as the antenna is connected with a coaxial cable. These currents lead to unwanted radiation from the coaxial cable itself which is why a quarter wave sleeve balun was used to isolate unwanted currents, as shown in Fig. 5. The balun was manufactured from a semi-rigid coaxial cable with a copper pipe connected to the coaxial shield. This structure provides a high isolation if the copper pipe has a length of about a quarter wavelength. Due to fringing fields at the open end of the copper pipe, the length of the balun was tuned to be shorter than a quarter wavelength according to the study of Saario et al.[29]. Thus, the length L_B of the balun was chosen to be 24 mm. The employed semi-rigid coaxial cable has a diameter of D_I =3.5 mm. As shown by Saario et al.[29], in general, a larger fraction D_O/D_I results in a larger isolation of the unwanted surface currents. However, the larger the diameter of the copper pipe, the larger the shadowing effect of the balun caused by the pipe and coaxial cable acting as a conducting scatterer/reflector[28]. Therefore, the diameter of the copper pipe was chosen to be $D_O =$ 10mm. The red line on the end of the coaxial cable marks the connection to the AUT. Note that the balun is only necessary if a coax cable is attached to the antenna for measurements.

The reflection coefficient was determined by measuring the AUTs S_{11} parameter. For the gain measurement, the AUT was placed on a turntable to measure gain patterns for azimuth and elevation angles regarding spherical coordinates. A reference antenna was placed at a distance $d > \frac{2D^2}{\lambda}$ with D being the largest dimension of the antenna. The scattering parameters S_{11}, S_{21}, S_{12} and S_{22} were measured and the gain of the AUT was calculated using the Friis transmission equation.

Results

An exemplary antenna was optimised with the proposed method for a Rogers RO4350B substrate with a relative permittivity of 3.66, a substrate thickness of 0.508 mm and a loss angle of 0.0037. The size of the ground plane was chosen to be 40 mm times 40 mm to feature enough space for future electronics of a WiFi sensor node to be embedded on the substrate. The geometric parameters chosen before optimisation as shown in Fig. 2 are listed in Table 2.

The optimisation converged within 26 generations and terminated with a fulfilled target value of below -17 dB reflection within the full specified band. The resulting antenna is presented in Fig. 6a and a close-up view of the optimised structure is shown in Fig. 6c. The fabricated prototype is seen in Fig. 6b. The antenna features an electrical size of $ka = 0.447$ and can therefore be considered a small antenna.

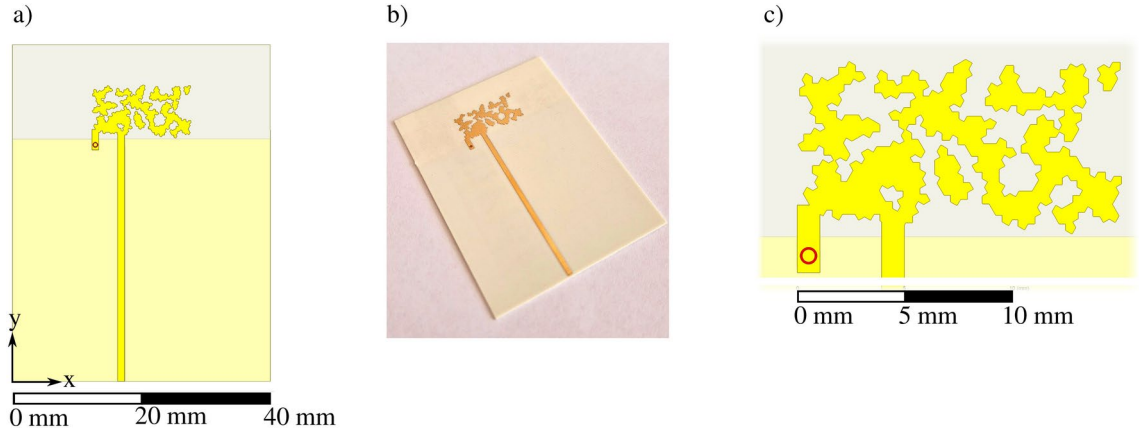

Fig. 6. The optimised antenna design is depicted with an overlaid coordinate system in (**a**), while (**b**) presents the actual manufactured prototype, and (**c**) zooms in on the intricate details of the optimised antenna features. Red circles highlight the vias that connect the shorting elements to the ground plane. Software used: Ansys[23], Inkscape[24].

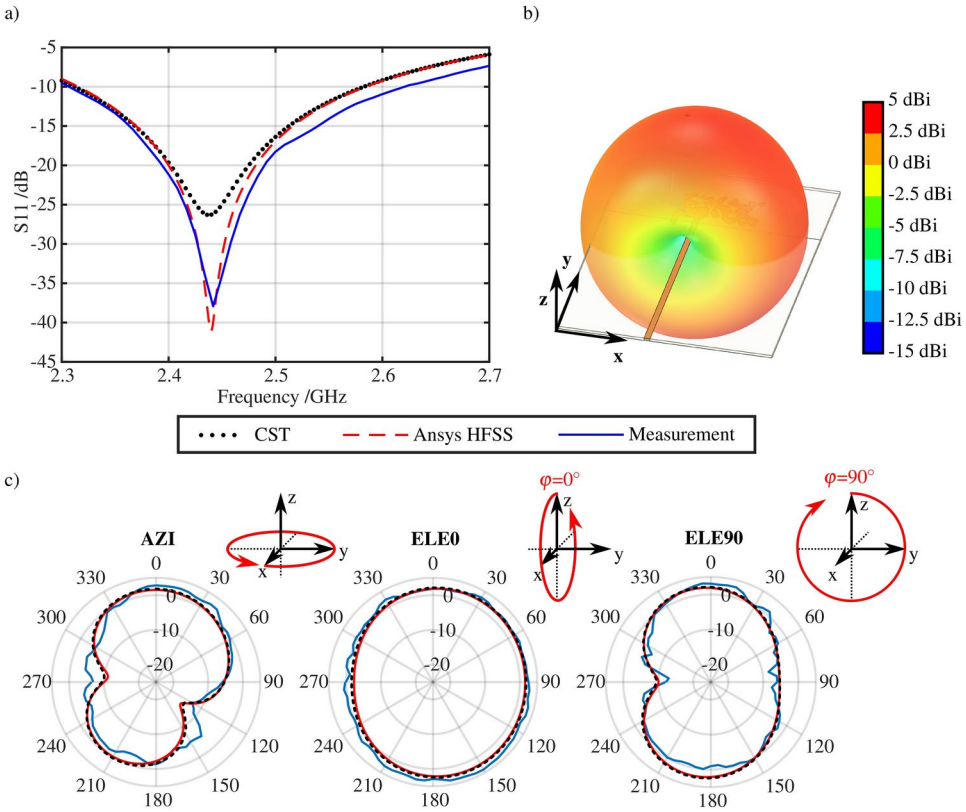

Fig. 7. (**a**) and (**c**) Depict a comparison of simulation results from CST (dotted black line) and Ansys HFSS (dashed red line) against actual measurements (solid blue line). (**a**) Shows the reflection coefficients, while (**b**) illustrates the 3D gain pattern of the antenna. (**c**) Presents the antenna's gain patterns at different orientations: azimuth (AZI, with $\vartheta = 90°$), and elevation at both $\varphi = 0°$ (ELE0) and $\varphi = 90°$ (ELE90). These are plotted according to the coordinate system defined in (**b**) and also in Fig. 6a. Software used: Ansys[23], CST[22], Matlab[21].

The scattering parameter S_{11} of the antenna is shown in Fig. 7a for simulations with CST (black dotted line) and Ansys HFSS (red dashed line) as well as measurement results (blue solid line). CST predicts a resonance frequency of 2.436 GHz with a reflection coefficient of − 26.29 dB, Ansys HFSS predicts a resonance frequency of 2.44 GHz at − 41 dB reflection and the measurement reveals a resonance frequency of 2.442 GHz with a reflection of − 37.93 dB. This means the maximum deviation between simulation and measurement concerning

resonance frequency is 0.16%. As observed earlier, the absolute values of the reflection coefficient can deviate between Ansys and CST[5].

The − 10 dB bandwidth obtained from CST is 270 MHz starting from 2.312 GHz up to 2.583 GHz, Ansys predicts a bandwidth of 270 MHz starting from 2.315 GHz up to 2.585 GHz and the measurement reveals a bandwidth of 308 MHz starting from 2.308 GHz up to 2.627 GHz. Within the—according to 802.11b/g/n/ax—full 2.4 GHz WiFi band a maximum reflection coefficient of, according to CST − 18.53 dB, Ansys − 19.5 dB and measurements − 21.4 dB is achieved.

The simulated 3D polar radiation pattern is displayed in Fig. 7b and the simulated and measured gain patterns are displayed in Fig. 7c from CST (black dotted line), Ansys (red dashed line), and measurement (blue solid line) for—in spherical coordinates—azimuth (AZI, with $\vartheta = 90°$), elevation at $\varphi = 0°$ (ELE0) and $\varphi = 90°$ (ELE90). The gain patterns agree visually very well with a mean absolute deviation (MAD) between Ansys and measurement of 1.94 dB for azimuth, 1.19 dB for elevation 0 and 1.25 dB for elevation 90 angles. The MAD between CST and measurement similarly has a value of 1.81 dB for azimuth, 0.87 dB for elevation 0, and 1.34 dB for elevation 90 angles. The simulation from CST predicts a maximum antenna gain of 2.69 dBi, Ansys HFSS predicts a maximum antenna gain of 2.63 dBi whereas the measurement reveals a maximum gain of 4.07 dBi. The difference in maximum Gain and the MAD can be explained by remaining surface current leaks causing radiation from the coaxial cable, between VNA and AUT, during measurements in the anechoic chamber, even though the balun structure is employed. This is explainable by the fact, that the ability of the balun to reduce surface current leaks is higher for larger fractions between D_O and D_I. However, too large diameters can distort the antenna as it places a large conducting structure in the proximity of the antenna.

To gain knowledge of the polarization the axial ratio is observed. The maximum axial ratio simulated with Ansys reveals 126.19 dB indicating a strong linear polarization.

Although the efficiency of the antenna was not measured, the simulation of Ansys predicts a radiation efficiency of 92.2% and the simulation of CST an efficiency of 96%. The agreement between measured and simulated gain supports these values. A loss analysis in Ansys reveals that of the observed 7.8% losses 2.39% originate from volume losses of the used substrate, 0.29% from the limited conductivity of the ground plane, and 4.98% from the limited conductivity of the antenna structure including the 50Ω feedline.

Furthermore, to understand the contribution to the radiation of the ground plane and to check if electronic components placed on the ground plane distort the antenna, the complex current density was simulated with Ansys HFSS. The results shown in Fig. 8 indicate, that the current density is highest within the antenna structure and only near to the antenna structure on the groundplane which is expected. Because the current density on the groundplane—although not zero—is much smaller than the current density on the antenna, electronic components placed above the ground plane should not alter the antenna's radiation pattern essentially.

To gain knowledge of the quality of the optimised antenna, two methods for calculating the theoretically maximum achievable antenna gain were used and the antenna was compared to previous studies. Compston et. al. presents the following formula for calculating the maximum gain:[30]

$$G_{\max} = \left(4\pi\frac{a}{\lambda}\right)^3 \sqrt{\frac{2}{1+(4\pi\frac{a}{\lambda})^2}} \tag{4}$$

Here, a is the radius of a sphere enclosing an antenna. Calculating the maximum gain reveals a value of − 1.23 dBi. For comparison, the gain equation derived by Harrington was used:[31]

$$G_{\max} = (ka)^2 + 2ka \tag{5}$$

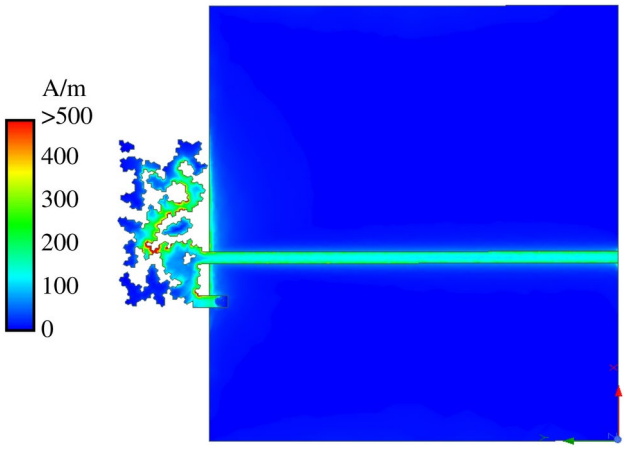

Fig. 8. Complex current density of antenna and ground plane simulated with Ansys HFSS. Software used: Ansys[23].

In this equation, a is again the radius of a sphere enclosing an antenna and k is the wavenumber $2\pi/\lambda$. For our size Eq. (5) calculates to 0.38 dBi. It is seen, that the proposed antenna with a measured maximum gain of 4.07 dBi surpasses both limits.

Therefore, the proposed antenna was compared to antennas of previous studies, antennas presented in application notes, antennas described in datasheets of commercially available antennas, and to a standard patch antenna as seen in Table 3.

The results from the comparison are as follows. Ullah et al.[32] developed a large pixelated patch antenna with an electrical size of $ka = 2.15$ operating at two frequencies. At 5.8 GHz it featured a bandwidth of 70 MHz with a gain of 4.7 dBi and an efficiency of 82%. Marasco et al.[1] used a classical patch antenna with a size of $ka = 1.38$ to compare his work of a pixelated patch. The efficiency of typical patches can be quite high up to $< 100\%$ depending on the employed substrate material and thickness which also affect its bandwidth. Higher bandwidth due to increased permittivity of the employed substrate or increased substrate thickness results in lower efficiency. E.g. the analysis of Pozar[39] presents, that the efficiency of patch antennas—that employ e.g. a substrate with a permittivity of $\varepsilon_r = 2.2$—can drop to below 80% if the thickness of the material is varied to acquire a bandwidth of 10% relative bandwidth. In the case of 2.45 GHz this translates to a 245 MHz absolute bandwidth. Marasco et al.[1] also published a flexible pixelated patch antenna. Although it has smaller dimensions than standard patch antennas, this comes at the cost of lower bandwidth and gain. Standard commercially available helical antennas[33] do achieve high gains but can also have lower efficiency. There are multiple studies, application notes, and commercially available IFA antennas in the size range of $ka = 0.34$ to $ka = 1.07$. However, their efficiency ranges from approximately 25–70%[35–38].

Observing the efficiency and antenna size values in Table 3 it is seen, that the antenna proposed in this work with an efficiency of 92.2% is superior to previous studies while at the same time featuring a small size of only $ka = 0.447$. Also the maximum S_{11} of − 21.4 dB within the full 2.4 GHz band is of very high quality. No comparisons of this value are listed in the table, as this value was not obtainable from most of the previous studies. The gain of the reported antenna is only lower compared to electrically large antennas with a size of $ka > 1$.

Conclusion and outlook

This study presents an innovative approach to the design and optimisation of pixelated inverted F-inspired antennas using genetic algorithms. The goal was to improve the performance of these antennas, making them more efficient and effective for modern wireless communication systems.

The results demonstrate significant advancements over traditional IFA designs. The optimised antenna achieved remarkable performance metrics, including a reflection coefficient of less than -21.4 dB across the full 2.4 GHz WiFi band, a bandwidth of 308 MHz, a measured gain of 4.07 dBi, and a simulated efficiency of 92.2%. These metrics indicate superior gain, efficiency, and impedance matching, highlighting the advantages of the genetic algorithm optimisation process.

A detailed loss analysis revealed the origin of losses, providing a basis for future improvements. While this study focused on an antenna designed for 2.4 GHz WiFi applications, the method is in principle applicable to any other frequency band.

The flexibility of this method is also noteworthy. While "Hat"-shaped Einstein tiles were used for demonstration purposes, the approach is versatile enough to accommodate various pixel shapes and design requirements. This adaptability makes it a valuable tool for antenna engineers looking to optimise different geometries and configurations.

In the future, antennas with even higher efficiency, multi-band antennas (e.g., for WiFi 6), high-gain antennas, and ultra-wideband antennas could be developed using the proposed method. For these purposes, multi-objective optimisation techniques as well as slotted or defected ground planes will be employed. Additionally,

Publication	Antenna	Electrical size of patch *ka*	Frequency GHz	Rel. bandwidth %	Gain dBi	Efficiency %
[32]	PixelPatch	2.15	5.2, 5.8	1.4	4.7	82
[1]	Patch	1.38	6	0.8	5.8	<100
[33]	Helical	1.21	2.45	4.1	4.5	82
[34]	IFA	1.07	2.45	3.3	2	> 70
[1]	Pixel Patch	0.89	3.96	0.4	1.89	n.a.
[35]	IFA	0.69	2.45	16.3	3.3	n.a.
[36]	IFA	0.39	2.45	12.2	2.65	n.a.
[36]	IFA	0.39	2.45	24.5	− 2.27	25
[37]	IFA	0.34	9.28	1.5	− 0.89	46
[38]	IFA	0.44	1.18	16.1	1.65	70
This work	Pixel IFA	0.447	2.45	12.6	4.07	92.2

Table 3. Comparison Table of different studies of small antennas and datasheets of commercially available antennas as well as antennas presented in application notes.

an IoT sensor node will be implemented on the antenna proposed in this work, as well as a single transistor matching setup for broadband communication.

Furthermore, the software created for this study will be used to design antennas with aperiodic patterns (e.g. generated from Einstein or Penrose tiling) and periodic patterns (e.g. with hexagon or rectangular tiles) and observe their impact on the performance of pixelated IFA-inspired antennas. Also the impact of geometric variations like tile size and feed and short offset will be observed in a parametric study.

In summary, this study introduces a robust and flexible optimisation framework for pixelated antennas, showcasing superior performance metrics and paving the way for future innovations in compact and efficient antenna designs. The success of this approach underscores its potential to revolutionize antenna design for modern communication systems.

Data availability

The data that support the findings of this study are available from the corresponding author, upon reasonable request.

Received: 2 August 2024; Accepted: 24 October 2024
Published online: 04 November 2024

References

1. Marasco, I. et al. A compact evolved antenna for 5g communications. *Sci. Rep.* **12**, 145. https://doi.org/10.1038/s41598-022-14447-9 (2022).
2. Mair, D., Unterladstaetter, M., Renzler, M. & Ussmueller, T. Evolutionary optimized pixelated antennas for 5g iot communication. In *2022 52nd European Microwave Conference (EuMC)* (2022).
3. Li, Y. et al. An automated approach for pixelated antenna topology design incorporating multi-objective optimization algorithms. In *2019 International Conference on Microwave and Millimeter Wave Technology (ICMMT)* (2019).
4. Jacobs, J. P. Accurate modeling by convolutional neural-network regression of resonant frequencies of dual-band pixelated microstrip antenna. *IEEE Antennas Wirel. Propag. Lett.* **20**, 2417–2421 (2021).
5. Mair, D. et al. Evolutionary optimized 3d wifi antennas manufactured via laser powder bed fusion. *IEEE Access* **11**, 121914–121923. https://doi.org/10.1109/ACCESS.2023.3328852 (2023).
6. Zechmeister, J., Lacik, J. & Kadlec, P. The design of pixelated siw horn antennas with nearly equal beamwidths using binary ink stamp optimization. *IEEE Access* **9**, 122216–122227 (2021).
7. Mair, D., Fischer, M., Konzilia, J., Renzler, M. & Ussmueller, T. Evolutionary optimization of antennas for structural health monitoring. *IEEE Access* **11**, 4905–4913. https://doi.org/10.1109/ACCESS.2023.3235896 (2023).
8. Gjokaj, V., Doroshewitz, J., Nanzer, J. & Chahal, P. A design study of 5g antennas optimized using genetic algorithms. In *2017 IEEE 67th Electronic Components and Technology Conference (ECTC)* (2017).
9. Ranjan, P., Choubey, A., Mahto, S. K. & Sinha, R. A six-band ultra-thin polarization-insensitive pixelated metamaterial absorber using a novel binary wind driven optimization algorithm. *J. Electromagn. Waves Appl.* **32**, 2367–2385 (2018).
10. Ghadimi, A., Nayyeri, V., Khanjarian, M., Soleimani, M. & Ramahi, O. M. A systematic approach for mutual coupling reduction between microstrip antennas using pixelization and binary optimization. *IEEE Antennas Wirel. Propag. Lett.* **19**, 2048–2052 (2020).
11. Lee, D. G., Jeong, T. & Hwang, K. C. Design of a wide-beamwidth pixelated dielectric resonator antenna using a modified stepped-impedance filter to suppress harmonics. *Appl. Sci.* **12**, 7765 (2022).
12. Karahan, E. A., Gupta, A., Khankhoje, U. K. & Sengupta, K. Deep learning based modeling and inverse design for arbitrary planar antenna structures at rf and millimeter-wave. In *2022 IEEE International Symposium on Antennas and Propagation and USNC-URSI Radio Science Meeting (AP-S/URSI)* (2022).
13. Sun, S., Jiang, Y. & Wang, J. Automatic design of pixelated near-zero refractive index metamaterials based on elite-preserving genetic algorithm optimization. *Results Phys.* **48**, 106461 (2023).
14. Qiao, T. et al. Pixel antenna optimization using the adjoint method and the method of moving asymptote. *IEEE Trans. Antennas Propag.* **71**, 2873–2878 (2023).
15. King, R., Harrison, C. & Denton, D. Transmission-line missile antennas. *IRE Trans. Antennas Propag.* **8**, 88–90. https://doi.org/10.1109/TAP.1960.1144802 (1960).
16. Waterhouse, R. Small microstrip patch antenna. *Electron. Lett.* **31**, 604. https://doi.org/10.1049/el:19950426 (1995).
17. Losito, O., Dimiccoli, V. & Barletta, D. Meander-line inverted f antenna designed using a transmission line model. In *The 8th European Conference on Antennas and Propagation (EuCAP 2014)* 1370–1373. https://doi.org/10.1109/EuCAP.2014.6902033 (2014).
18. Elsheakh, D. M. & Abdallah, E. A. Multiband printed-ifa on electromagnetic band-gap ground plane. In *Proceedings of the 2012 IEEE International Symposium on Antennas and Propagation* 1–2. https://doi.org/10.1109/APS.2012.6348738 (2012).
19. Alnas, J., Giddings, G. & Jeong, N. Bandwidth improvement of an inverted-f antenna using dynamic hybrid binary particle swarm optimization. *Appl. Sci.* **11**, 47. https://doi.org/10.3390/app11062559 (2021).
20. Smith, D., Myers, J. S., Kaplan, C. S. & Goodman-Strauss, C. An aperiodic monotile. *arXiv 2303.10798* 1–89 (2023).
21. The Mathworks Inc., MATLAB, Version R2023a. https://www.mathworks.com/products/matlab.html (2023).
22. Dassault Systèmes, CST Studio Suite, Version 2022.05. https://www.3ds.com/products/simulia/cst-studio-suite (2022).
23. ANSYS, Inc., ANSYS Electronics Desktop, Version 2023R2. https://www.ansys.com/products/electronics (2023).
24. Inkscape Project, Inkscape, Version 1.3 (0e150ed6c4, 2023-07-21). https://inkscape.org/ (2023).
25. Schirmann, J., Franca, S., Flicker, F. & Grushin, A. G. Tile generator (2024, accessed 6 Apr 2024). https://cs.uwaterloo.ca/csk/spectre/app.html.
26. Goldberg, D. E. *Genetic Algorithms in Search, Optimization, and Machine Learning* (Addison-Wesley, 1989).
27. Massey, P. & Boyle, K. Controlling the effects of feed cable in small antenna measurements. In *Twelfth International Conference on Antennas and Propagation, 2003 (ICAP 2003). (Conf. Publ. No. 491), vol. 2* 561–564. https://doi.org/10.1049/cp:20030137 (2003).
28. Icheln, C., Krogerus, J. & Vainikainen, P. Use of balun chokes in small-antenna radiation measurements. *IEEE Trans. Instrum. Meas.* **53**, 498–506. https://doi.org/10.1109/TIM.2004.823299 (2004).
29. Saario, S. A., Lu, J. W. & Thiel, D. V. Full-wave analysis of choking characteristics of sleeve balun on coaxial cables. *Electron. Lett.* **38**, 304–305. https://doi.org/10.1049/el:20020227 (2002).
30. Compston, A. J., Fluhler, J. D. & Schantz, H. G. A fundamental limit on antenna gain for electrically small antennas. In *2008 IEEE Sarnoff Symposium* 1–5. https://doi.org/10.1109/SARNOF.2008.4520113 (2008).
31. Harrington, R. F. Effect of antenna size on gain, bandwidth, and efficiency. *J. Res. Nat. Bur. Stand* **64**, 1–12. https://doi.org/10.6028/jres.064D.003 (1960).
32. Ullah, M. A., Keshavarz, R., Abolhasan, M., Lipman, J. & Shariati, N. Multiservice compact pixelated stacked antenna with different pixel shapes for iot applications. *IEEE Internet Things J.* **10**, 19883–19897. https://doi.org/10.1109/JIOT.2023.3281816 (2023).

33. LinxTechnologies. Ant-2.4-pw-lpn 2.4 ghz compact helical antenna (2024, accessed 18 May 2024). https://www.mouser.at/datasheet/2/418/9/ENG_DS_L9000099_01_B-3238970.pdf.
34. LairdConnectivity. 2.4 ghz flexpifa antenna (2024, accessed 18 May 2024). https://www.ezurio.com/documentation/datasheet-24-ghz-flexpifa.
35. TexasInstruments & Audun, A. Application note an043 small size 2.4 ghz pcb antenna (2024, accessed 18 May 2024). https://www.ti.com/lit/an/swra117d/swra117d.pdf.
36. NXP. Compact planar antennas for 2.4 ghz communication (2024, accessed 18 May 2024). https://www.nxp.com/docs/en/application-note/AN2731.pdf.
37. Lee, S. & Sung, Y. Reconfigurable pifa with a parasitic strip line for a hepta-band wwan/lte mobile handset. *IET Microwaves Antennas Propag.* **9**, 108–117. https://doi.org/10.1049/iet-map.2014.0451 (2015).
38. Bousselmi, A., Gharsallah, A. & Vuong, T. P. Design and implementation of a tri-band miniaturized planar inverted-f antenna with double resonator for gps application. *Technol. Appl. Sci. Res.* **9**, 4980 (2019).
39. Pozar, D. Microstrip antennas. *Proc. IEEE* **80**, 79–91. https://doi.org/10.1109/5.119568 (1992).

Acknowledgements

This research was funded by the Universität Innsbruck. The authors would like to thank Andreas Hanschek, Samuel Pröll, Simon Marxgut and Viktor Steixner for their review of this manuscript and Clemens Zierhofer for his support.

Author contributions

D.M. conceived the research idea, designed the study, conducted the experiments, analyzed and interpreted the data, and wrote the initial draft of the manuscript. D.B. interpreted the data and substantively revised the manuscript. All authors reviewed the manuscript.

Competing interests

The authors declare no competing interests.

Additional information

Correspondence and requests for materials should be addressed to D.M.